Geological Survey of Sweden

Age of volcanism in the ore districts of Persberg, Långban and Nordmark

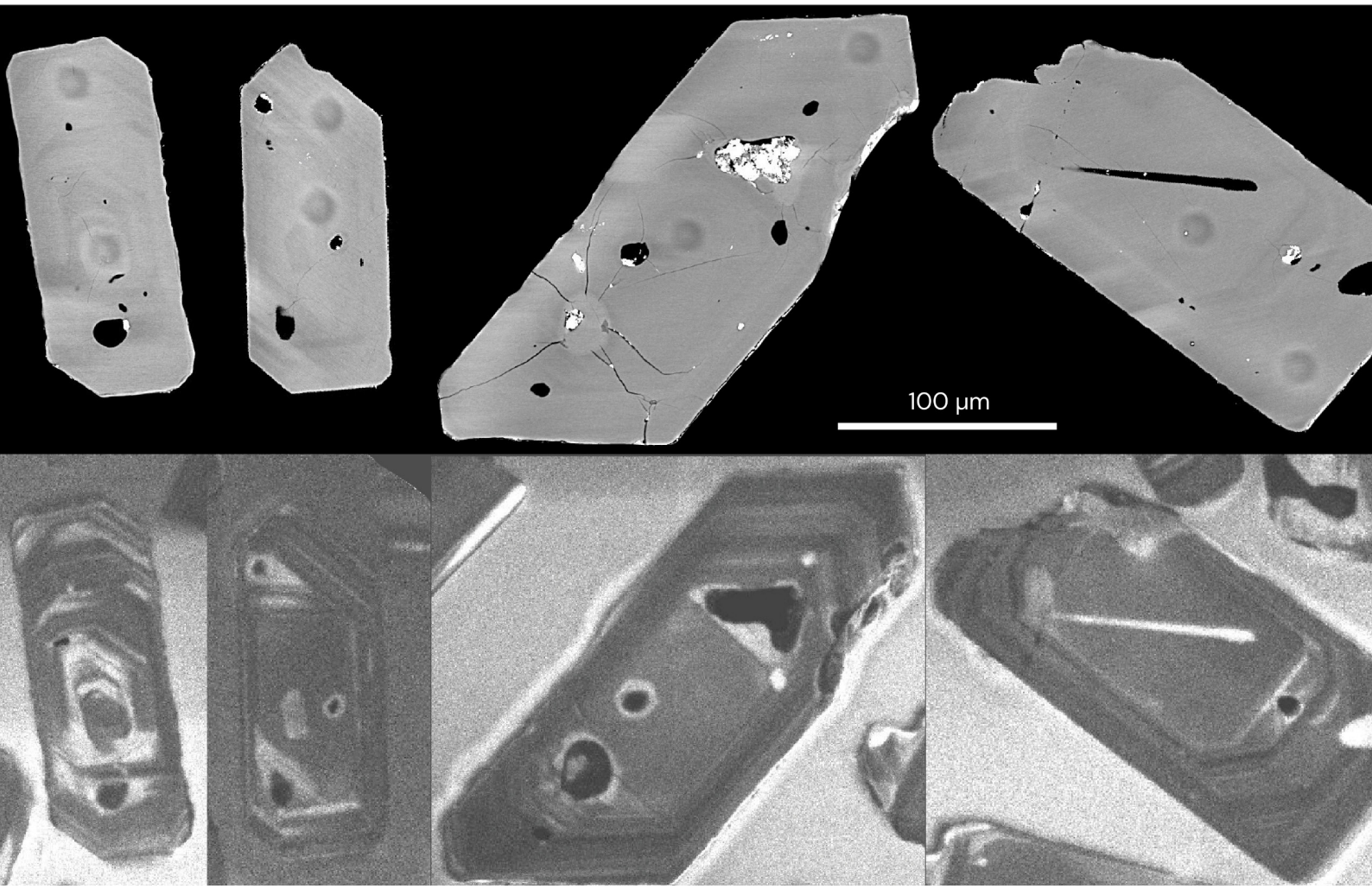

Stefan Andersson & George Morris

www.sgu.se

SGU-rapport 2026:02

Authors: Stefan Andersson & George Morris
Reviewed by: Pauline Jeanneret
Head of unit: Ildiko Antal Lundin/Kaj Lax
Editor: Lina Rönnåsen

Cover photo: Back-scattered electron images (BSE) and cathodoluminescence images (CL) of zircons from a metarhyolite from the Persberg ore district.
Photographer: George Morris

April 2026

Geological Survey of Sweden
Box 670, 751 28 Uppsala
phone: 018-17 90 00
e-mail: sgu@sgu.se
www.sgu.se

Content

Abstract

The Geological Survey of Sweden has performed zircon U–Pb geochronology of coherent metarhyolitic wall rocks associated with the marble-hosted skarn iron oxide ores in the historically important Swedish ore districts of Persberg, Långban, and Nordmark in western Bergslagen. The primary aims of the study were to establish the timing of volcanic activity across the districts and assess potential age differences between them. This work also tests the hypothesis that Mn-poor and Mn-rich skarn types could have formed within the same stratigraphic level in the volcanic–sedimentary succession, a hypothesis proposed based on recent fieldwork that identified similar primary volcanic textures in the host and wall rocks throughout the studied area. The new age data further contribute to refining the volcanic framework of the westernmost Bergslagen ore province, thereby improving our understanding of its geological evolution.

U–Pb zircon analyses acquired by secondary ion mass spectrometry (SIMS) yielded concordia ages of 1892.5 ± 4 Ma (Persberg), 1889.5 ± 4.5 Ma (Långban), and 1887.5 ± 5 Ma (Nordmark). These results demonstrate broadly coeval felsic volcanism across the districts, indicating no meaningful stratigraphic separation among them. The data support the interpretation of a shared, proximal volcanic–sedimentary ore-forming environment active around 1.89 Ga, contemporaneous with plutonic-subvolcanic activity in the region. The study thereby refines the regional volcanic framework and strengthens the genetic links between skarn mineralisation and the ca 1.89 Ga volcanic stage across Bergslagen.

Sammanfattning

Sveriges geologiska undersökning (SGU) har utfört åldersbestämningar med hjälp av zirkon från vulkaniska bergarter associerade med olika typer av skarnjärnmalm från de historiskt viktiga svenska malmdistrikten Persberg, Långban och Nordmark i västra Bergslagen. Huvudsyftet med studien var att undersöka när den vulkaniska aktiviteten i området ägt rum samt om det finns åldersskillnader mellan distrikten. Dessutom testas hypotesen om manganfattiga och manganrika skarnmalmtyper bildats inom samma stratigrafiska nivå i den vulkaniska–sedimentära lagerföljden. Hypotesen baseras på nyligen genomförda fältarbeten i området som påvisat flera likheter i den primära vulkaniska texturen hos både värd- och sidobergarterna till skarnjärnmalmerna. Nya åldersdata för bildningen av olika bergarter i västra Bergslagen är dessutom viktigt för att förbättra förståelsen av områdets geologiska utveckling.

Zirkondatering med uran–blymetoden, analyserad med jonmasspektrometri (eng. *secondary ion mass spectrometry, SIMS*) gav konkordiaåldrar på 1892,5 ± 4 Ma (Persberg), 1889,5 ± 4.5 Ma (Långban) och 1887,5 ± 5 Ma (Nordmark). Resultaten indikerar att den vulkaniska aktiviteten i de tre distrikten i stort sett var samtidig och att det inte finns någon betydande stratigrafisk skillnad mellan dem. Detta stödjer tolkningen att skarnjärnmalmerna bildades i en gemensam vulkanisk–sedimentär miljö, samt att malmbildningen sammanföll med plutonisk–subvulkanisk magmatism i regionen. Studien bidrar därför till ökad förståelse av den regionala vulkaniska aktiviteten och förstärker kopplingen mellan skarnmineralisering och den omfattande vulkaniska fas som ägde rum för ca 1,89 miljarder år sedan i hela Bergslagen.

Introduction

The historically significant ore districts of Persberg, Långban, and Nordmark lie in the westernmost part of the historic Bergslagen ore province, near the boundary between the Bergslagen and Sveconorwegian lithotectonic units (fig. 1). In this area, skarn iron oxide deposits occur within marble horizons that are embedded in a predominantly felsic volcanic–volcanosedimentary succession (Törnebohm 1875; Petersson 1896; Sjögren 1910; Magnusson 1925, 1929, 1930; Boström et al. 1979; Jonsson 2004; Andersson et al. 2025).

The Bergslagen ore province, a major domain within the Svecokarelian orogen of the Fennoscandian Shield, is composed of intrusive rocks enclosing a metasupracrustal sequence. The intrusions include an early suite of granitoids, diorite, and gabbro (GDG) dated to ca 1.91–1.87 Ga, and two younger suites of granite, granodiorite, syenitoid, quartz monzodiorite, and gabbro (GSDG) formed at ca 1.87–1.84 Ga and 1.81–1.78 Ga (Stephens et al. 2009; Stephens & Jansson 2020). The latter GSDG suite dominates the westernmost Bergslagen region (fig. 1). The GDG suite intruded into a ca 1.91–1.88 Ga supracrustal sequence comprising mainly rhyolitic volcanic rocks, subordinate mafic volcanics, and interbedded siliciclastic sedimentary rocks. Calcitic to dolomitic marble horizons are intercalated with the volcanic units (Stephens et al. 2009; Stephens & Jansson 2020). This succession is interpreted to have formed in an extensional back-arc setting adjacent to an active continental margin (Allen et al. 1996). Both the supracrustal rocks and the younger intrusions were subsequently affected by polyphase ductile deformation and regional low-pressure, amphibolite facies metamorphism during the ca 1.9–1.8 Ga Svecokarelian orogeny (Stephens et al. 2009). Largely undeformed ca 1.85–1.75 Ga granite–pegmatite intrusions also occur in the Bergslagen province but are rare in the westernmost part.

The three ore districts exhibit distinct types of skarn iron oxide mineralisation. The Persberg district is characterised by Mn-poor, magnetite-dominated pyroxene-garnet-amphibole skarns, with subordinate quartz-rich or anthophyllite-talc skarn ores (Magnusson 1925). In contrast, the Långban district hosts Mn-rich skarn ores dominated by hausmannite and braunite, along with other Mn-bearing silicates, which occur alongside Mn-poor magnetite-hematite ores associated with pyroxene-amphibole-garnet-olivine skarns (Magnusson 1930). The Nordmark district, similar to Persberg, mainly comprises Mn-poor, magnetite-dominated pyroxene-garnet-amphibole skarns (Magnusson 1929), although Mn-rich skarn ores with hausmannite are locally present in the Jakobsberg and Nordmark ore fields (Magnusson 1929). The Mn-rich skarn ores of the so-called Långban-type have been interpreted as syn-sedimentary exhalative deposits formed in a shallow submarine environment (Boström et al. 1979; Holtstam & Mansfeld 2001).

► **Figure 1.** Geological map of the westernmost part of the Bergslagen ore province, at the border between the Bergslagen and Sveconorwegian lithotectonic units. The dotted pattern depicts porphyritic or porphyroblastic rocks, and the diagonal striped pattern hydrothermally altered rocks. The map also shows the analysed localities (Persberg, Långban and Nordmark) along with other relevant zircon U–Pb ages reported in the literature (Welin 1987; Andersen et al. 2009; Stephens et al. 2009; Kuipers et al. 2018). The map is based on the revised 1:50 000–1:250 000 geological map of SGU (Andersson et al. 2025). The inset map to the lower left shows the lithotectonic units and major deformation zones in southcentral Sweden, based on the 1: 1 000 000 geological map of SGU (Bergman et al. 2012). The coordinate system is SWEREF 99 TM.

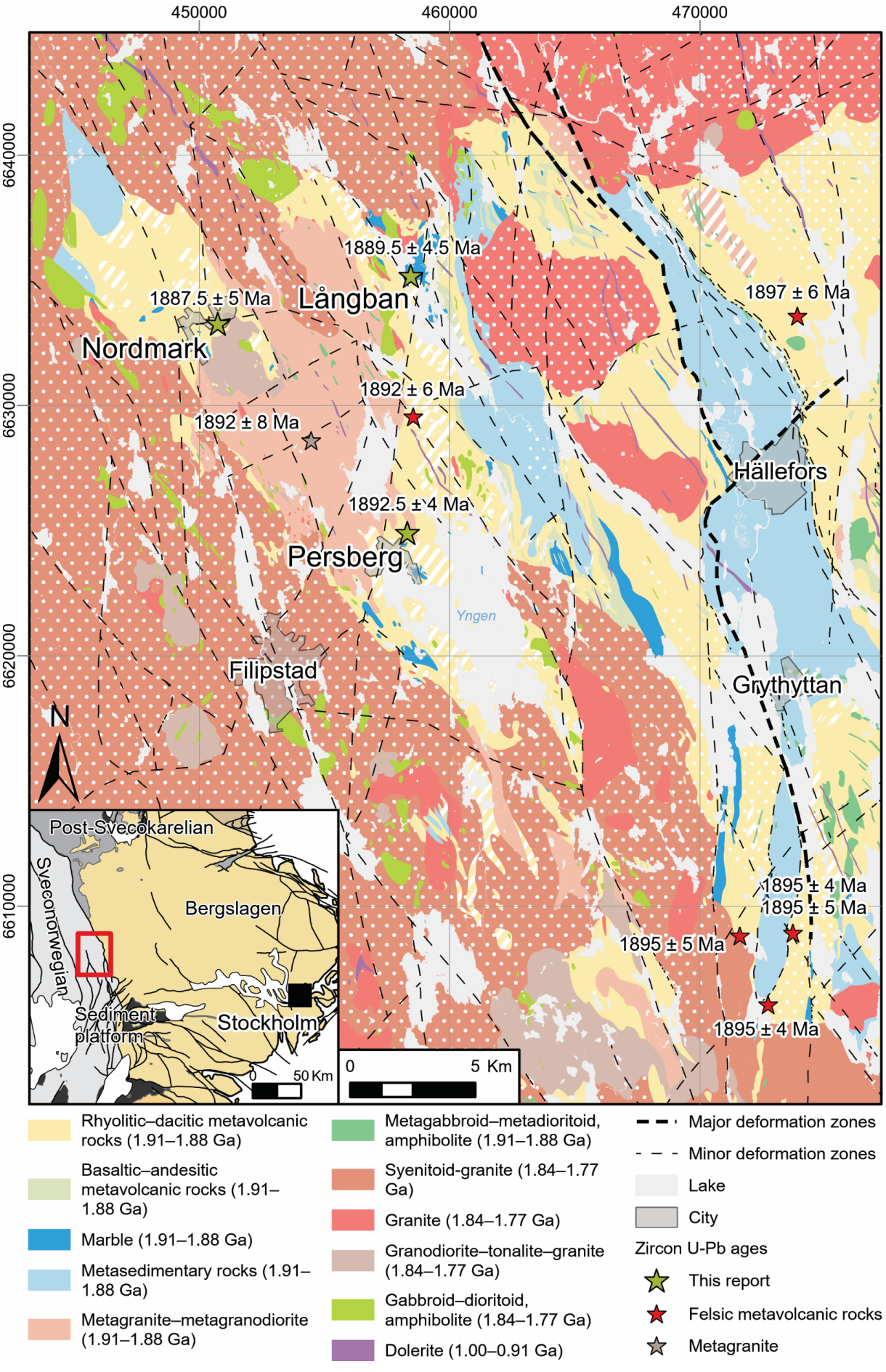
450000
460000
470000
6640000
6630000
6620000
6610000
1889.5 ± 4.5 Ma
1887.5 ± 5 Ma
Långban
Nordmark
1897 ± 6 Ma
1892 ± 6 Ma
1892 ± 8 Ma
Hällefors
1892.5 ± 4 Ma
Persberg
Yngen
Filipstad
Grythyttan
N
1895 ± 4 Ma
1895 ± 5 Ma
1895 ± 5 Ma
1895 ± 4 Ma
Post-Svecokarelian
Sveconorwegian
Bergslagen
Sediment platform
Stockholm
0 50 Km
0 5 Km
Rhyolitic–dacitic metavolcanic rocks (1.91–1.88 Ga)
Basaltic–andesitic metavolcanic rocks (1.91–1.88 Ga)
Marble (1.91–1.88 Ga)
Metasedimentary rocks (1.91–1.88 Ga)
Metagranite–metagranodiorite (1.91–1.88 Ga)
Metagabbroid–metadioritoid, amphibolite (1.91–1.88 Ga)
Syenitoid-granite (1.84–1.77 Ga)
Granite (1.84–1.77 Ga)
Granodiorite–tonalite–granite (1.84–1.77 Ga)
Gabbroid–dioritoid, amphibolite (1.84–1.77 Ga)
Dolerite (1.00–0.91 Ga)
Major deformation zones
Minor deformation zones
Lake
City
Zircon U-Pb ages
This report
Felsic metavolcanic rocks
Metagranite

The volcanic wall rocks and associated skarn ores and marble horizons in these districts have traditionally been assigned to either a lower or upper stratigraphic interval. The Na-rich volcanic rocks of Persberg were considered stratigraphically lower, while the K-rich volcanic rocks of Långban were assigned to a higher unit (Magnusson 1925, 1930; Björk 1986). Volcanic rocks in Nordmark display a broader compositional range, with both Na- and K-enriched signatures (Andersson et al. 2025). These chemical differences were initially interpreted as primary magmatic features but are now recognised as products of hydrothermal alteration associated with volcanic activity, which overprints the original compositions (e.g., Stephens et al. 2009; Jansson & Stephens 2020; Andersson et al. 2025, and references therein). Stratigraphic divisions based solely on Na- or K-rich compositions are therefore no longer considered valid. An alternative interpretation suggests that the Na- and K-altered metavolcanic rocks may still represent different stratigraphic levels, with alteration occurring at varying depths, where deeper Na alteration overprinted earlier K alteration in proximity to mafic intrusions (cf. Stephens et al. 2009).

Recent field investigations by Andersson et al. (2025) identified numerous similarities in the primary features and volcanic textures of the wall rocks across the three districts. This observation suggests that these areas may not represent distinct stratigraphic levels, but rather equivalent positions within a single volcanic–sedimentary succession.

To test this hypothesis, coherent volcanic units adjacent to the skarn iron ores in all three districts were sampled for zircon U–Pb geochronology. The objectives were to determine the timing of volcanic activity in each district, assess potential age differences, and evaluate whether the Mn-poor and Mn-rich skarn ores could have formed within a shared stratigraphic interval. Furthermore, the westernmost part of the Bergslagen ore province lacks high-precision age constraints on volcanic rocks, emphasising the importance of acquiring new geochronological data to refine the regional volcanic framework and improve our understanding of the province's geological evolution.

Sampling and analytical method

One sample from each of the three ore districts was collected for U–Pb zircon dating at the NORDSIM facility of the Swedish Natural History Museum in Stockholm. The sampling targeted metarhyolitic volcanic rocks interpreted as coherent in origin and occurring adjacent to the main skarn-bearing volcanic–sedimentary sequences.

Zircons were extracted from a crushed rock sample using a Wilfley water table. Magnetic minerals were removed with a hand magnet. Handpicked crystals were mounted in transparent epoxy resin together with chips of primary reference zircon 91500 and secondary reference zircons OGC and M257. The zircon mounts were polished and, after gold coating, examined by Cathodoluminescence (CL) imaging using the scanning electron microscope at the Swedish Museum of Natural History in Stockholm.

U–Pb zircon geochronology was carried out with high-spatial resolution secondary ion mass spectrometer (SIMS) analysis using the Cameca IMS 1280 at the NORDSIM facility in March 2025. Detailed descriptions of the analytical procedures are given in Whitehouse et al. (1997, 1999), and Whitehouse & Kamber (2005). A ca 6 nA O_2^- primary ion beam was used, yielding spot sizes of ca 10–15 μm. The U/Pb ratios, elemental concentrations and Th/U ratios were calibrated relative to the Geostandards zircon 91500 reference, which has an age of ca 1065 Ma (Wiedenbeck et al. 1995, 2004). Common Pb corrected isotope values were calculated using the modern common Pb composition (Stacey & Kramers 1975) and measured ^{204}Pb when the ^{204}Pb count rate was above the detection limit. Decay constants follow the recommendations of Steiger & Jäger (1977). Diagrams and age calculations of isotopic data were made using the *IsoplotR*

toolbox (Vermeesch 2018). All spot data are presented in Appendices 1–3. Age uncertainties for concordia plots are presented at the 2σ or 95% confidence level. After analysis, back-scattered electron (BSE) images of the dated zircons were taken using the scanning electron microscope at the Swedish Museum of Natural History in Stockholm, to confirm the exact location of the analysed spots.

Sample description

The following section presents the characteristics of the outcrops and samples targeted in this study.

SAN230139A, Persberg

Sample SAN230139A was collected from an outcrop featuring metarhyolite near the Hallgruvorna ore field (SWEREF coordinates: 6624911/458314) in the northern part of the Persberg ore district (fig. 1). The sampled outcrop consists of a grey, foliated, quartz- and feldspar-phyric metarhyolite (fig. 2A–B). This porphyritic metarhyolite occurs adjacent to, or possibly intrudes, a skarn-altered metarhyolitic volcanic siltstone–sandstone, which is the main wall rock to the marble and skarn horizons in the district. The foliated character likely originates from overprinting and localised deformation.

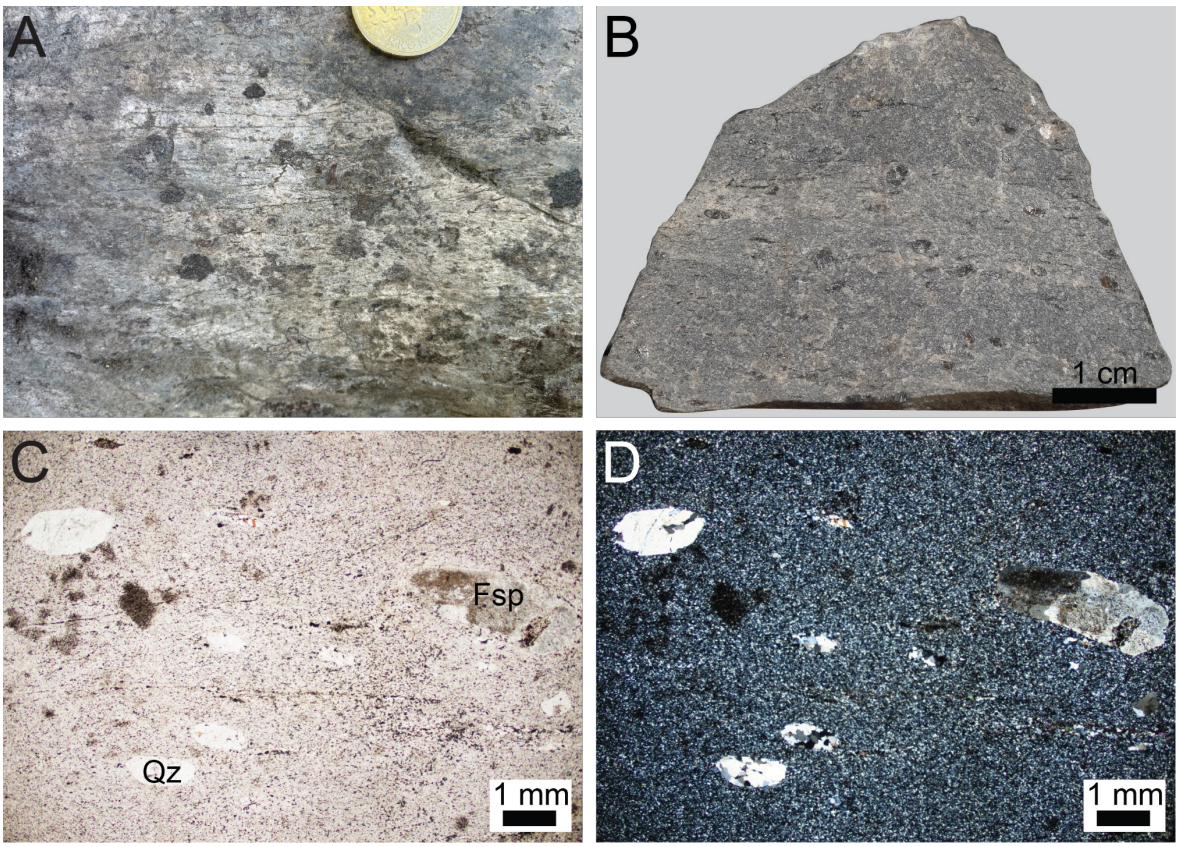

Figure 2. A. Photo of the sampled outcrop showing a grey foliated metarhyolite. Persberg district. **B.** Photo of sample SAN230139A. **C–D.** Euhedral to rounded quartz phenocrysts and euhedral feldspar in a fine-grained groundmass. Thin section EJ-243 (Observation SAN230139). Single-polarised light in C and cross-polarised light in D. Mineral abbreviations: Fsp = feldspar, Qz = quartz. Photos: Stefan Andersson.

The groundmass ranges from 10 to 50 μm and is composed of quartz, feldspar, muscovite, and partly chloritised biotite. Phenocrysts of quartz and plagioclase range in size from 0.5 to 4 mm. Feldspar phenocrysts are generally euhedral, while quartz phenocrysts are typically elongated or rounded (fig. 2C–D). Phenocrysts are evenly distributed throughout the sample. Accessory minerals include magnetite and zircon. Based on its texture and mineralogical composition, the sampled volcanic rock is interpreted as a coherent lava.

Lithochemical data, obtained by ALS Global using Fusion decomposition followed by inductively coupled plasma atomic emission spectroscopy (ICP-AES) analysis, show the following major element concentrations (Andersson et al. 2025): 77.6 wt% SiO_2, 11.5 wt% Al_2O_3, 3.80 wt% Na_2O, 3.82 wt% K_2O, 0.41 wt% CaO, 2.48 wt% Fe_2O_3 and 0.46 wt% MgO. These results, together with the mineralogical characteristics, indicate that the sampled metarhyolite is largely unaltered in contrast to nearby rocks affected by a combination of Na- and Fe–Mg-alteration or skarn alteration (Andersson et al. 2025).

The extracted zircon grains are subhedral to euhedral, displaying elongate prismatic shapes (fig. 3). They range from approximately 60 to 280 μm in length and 40 to 100 μm in width. Many zircons display core-rim structures, with distinct unzoned cores and oscillatory-zoned overgrowths. Several zircon crystals contain small (<20 μm) inclusions of quartz, fluorapatite, and xenotime.

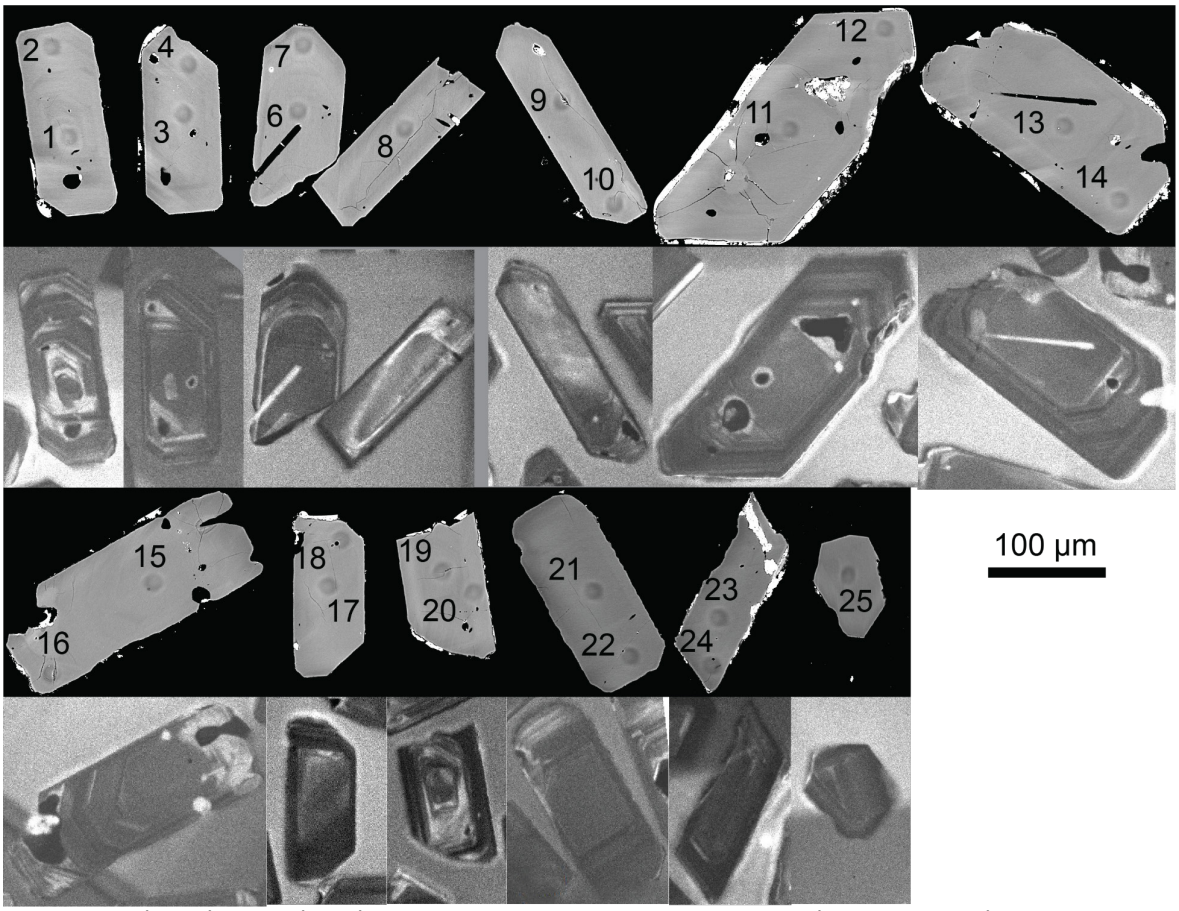

Figure 3. BSE (upper) and CL (lower) images of zircons from sample SAN230139A (Persberg district) with marked analytical points. Brightest white in the BSE images is remnants of the gold coating. Spot 5 was not imaged by BSE because of large errors. Photos: George Morris.

SAN240130A, Långban

Sample SAN240130A was collected from a metarhyolite in the Långban ore district, south of the main mines (fig. 1; SWEREF coordinates: 6635175/458453). The sampled outcrop comprises a grey to greyish-red, quartz-phyric metarhyolite in contact with skarn-altered marble. The metarhyolite contains cross-cutting, green to black, centimetre-sized veins and patches representing skarn alteration (fig. 4A–B). The collected sample was, however, taken from a part of the outcrop devoid of such features. This rock exposure has also been described by Magnusson (1925; sample Nr.8, p. 47–50) and Björk (1986; sample LB78: 274).

The groundmass is typically 100–200 μm in grain size but becomes finer-grained (< 20 μm) in some domains, particularly around the quartz phenocrysts. It mainly consists of quartz and feldspar, with alkali feldspar dominating, together with minor green to brown biotite. Quartz phenocrysts reach up to 2 mm in size, commonly occurring in clusters and displaying euhedral to subhedral forms, often with embayed outlines (fig. 4C–D). Separation of quartz-rich and alkali feldspar-rich domains is clearly visible in hand specimen as irregular to rounded patches (fig. 4B), a feature also noted by Magnusson (1925; p. 50). Accessory minerals include an allanite-group mineral, magnetite, and zircon. Based on its texture and mineralogy, the sampled volcanic rock is interpreted as a coherent lava.

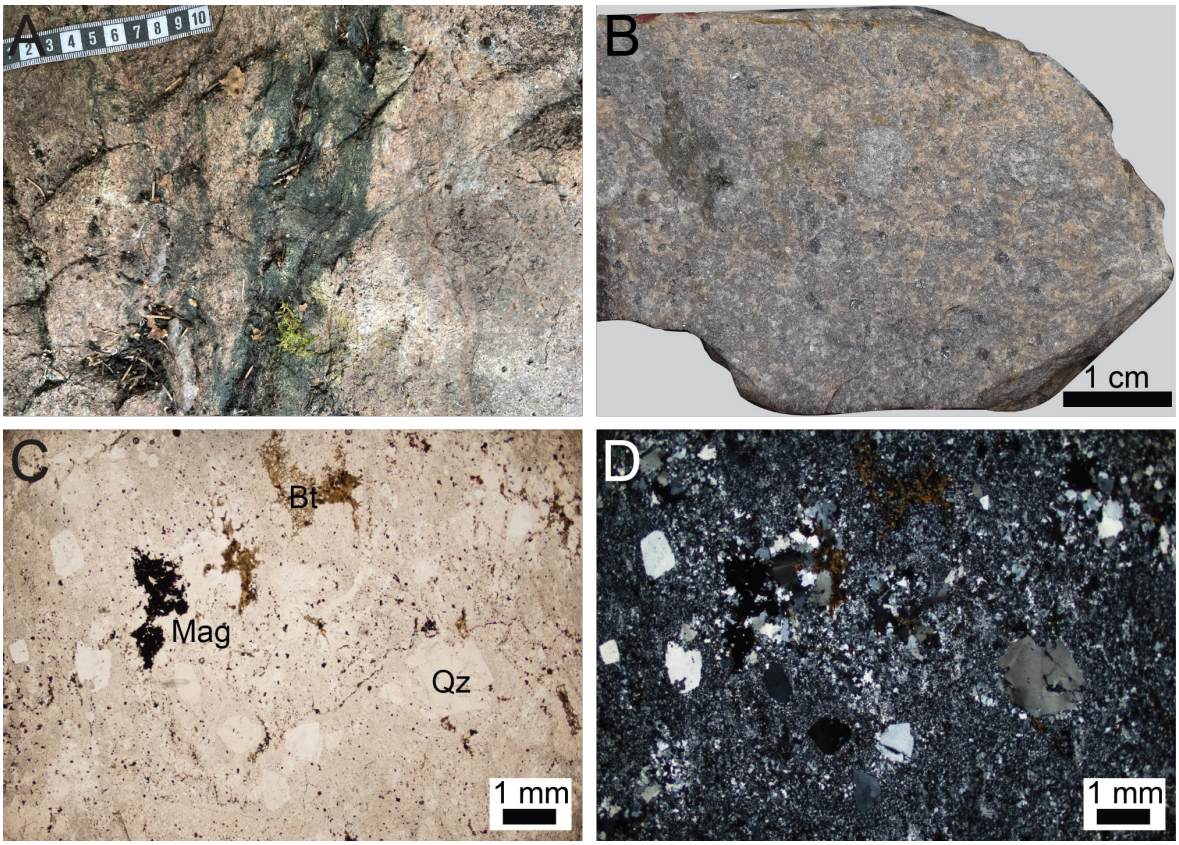

Figure 4. A. Photo of the sampled outcrop showing grey to red metarhyolite with green to black skarn veins and patches. Långban district. **B.** Photo of sample SAN240130A. **C–D.** Variably sized quartz phenocrysts with embayment texture (lower right) in a groundmass with varying grain size. Thin section LB78: 274. Single-polarised light in C and cross-polarised light in D. Mineral abbreviations: Bt = biotite, Mag = magnetite, Qz = quartz. Photos: Stefan Andersson.

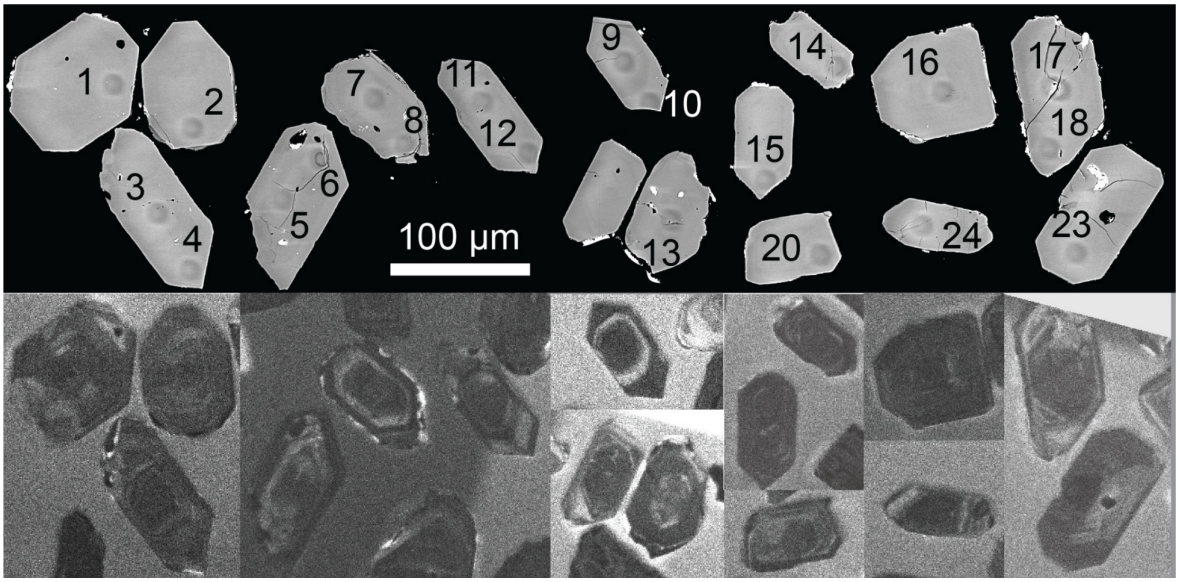

Figure 5. BSE (upper) and CL (lower) images of zircons from sample SAN240130A (Långban district) with marked analytical points. Brightest white in the BSE images is remnants of the gold coating. Spots 19, 21, 22 and 25 were not imaged by BSE. Photos: George Morris.

Lithochemical data, obtained by ALS Global using Fusion decomposition followed by ICP-AES analysis, show the following major element concentrations (Andersson et al. 2025): 77.6 wt% SiO_2, 10.5 wt% Al_2O_3, 0.19 wt% Na_2O, 8.66 wt% K_2O, 0.81 wt% CaO, 2.34 wt% Fe_2O_3 and 0.71 wt% MgO. These data, together with the mineralogical and textural features, indicate that the metarhyolite is strongly K-altered and affected by skarn alteration.

The extracted zircon grains are subhedral to euhedral, with elongate to stubby prismatic morphologies (Fig. 5). They range from approximately 60 to 120 µm in length and 30 to 80 µm in width. Most zircons display oscillatory zoning, characterised by CL-dark cores surrounded by CL-brighter overgrowths.

SAN240131A, Nordmark

Sample SAN240131A was collected from a metarhyolite from an older mining shaft in the Nordmark ore district (fig. 1; SWEREF coordinates: 6633268/450744). The sampled rock comprises a quartz- and feldspar-phyric metarhyolite (fig. 6A–B) and represents the same volcanic unit that continues south-eastwards towards the Nordmark ore field (Swe. *Nordmarks odalfält*). A sample from this unit was also collected during the mapping project that formed the basis for SGU's Af map series (Björk 1986; sample LB77:46).

Petrographic examination of both samples shows that the groundmass consists of quartz, alkali feldspar, plagioclase, biotite, and minor muscovite. The grain size ranges from 10 to 100 µm. Quartz phenocrysts reach ca 3 mm in size and display subrounded to rounded, partly recrystallised grains with embayed margins (fig. 6C–D). Plagioclase phenocrysts are up to 2 mm in size, subhedral to euhedral, rectangular in shape, and show both Carlsbad and polysynthetic twinning. They commonly contain abundant inclusions, mainly of muscovite. The phenocrysts occur either as isolated grains or in distinct clusters. Mafic minerals, primarily biotite, commonly form aggregates that define a weak foliation. Associated minerals within these aggregates include muscovite, zoned epidote-allanite aggregates, zircon, and monazite and/or titanite. Magnetite occurs disseminated with grains up to 200 µm in size. Based on its mineralogy and texture, the sampled volcanic rock is interpreted as a coherent lava.

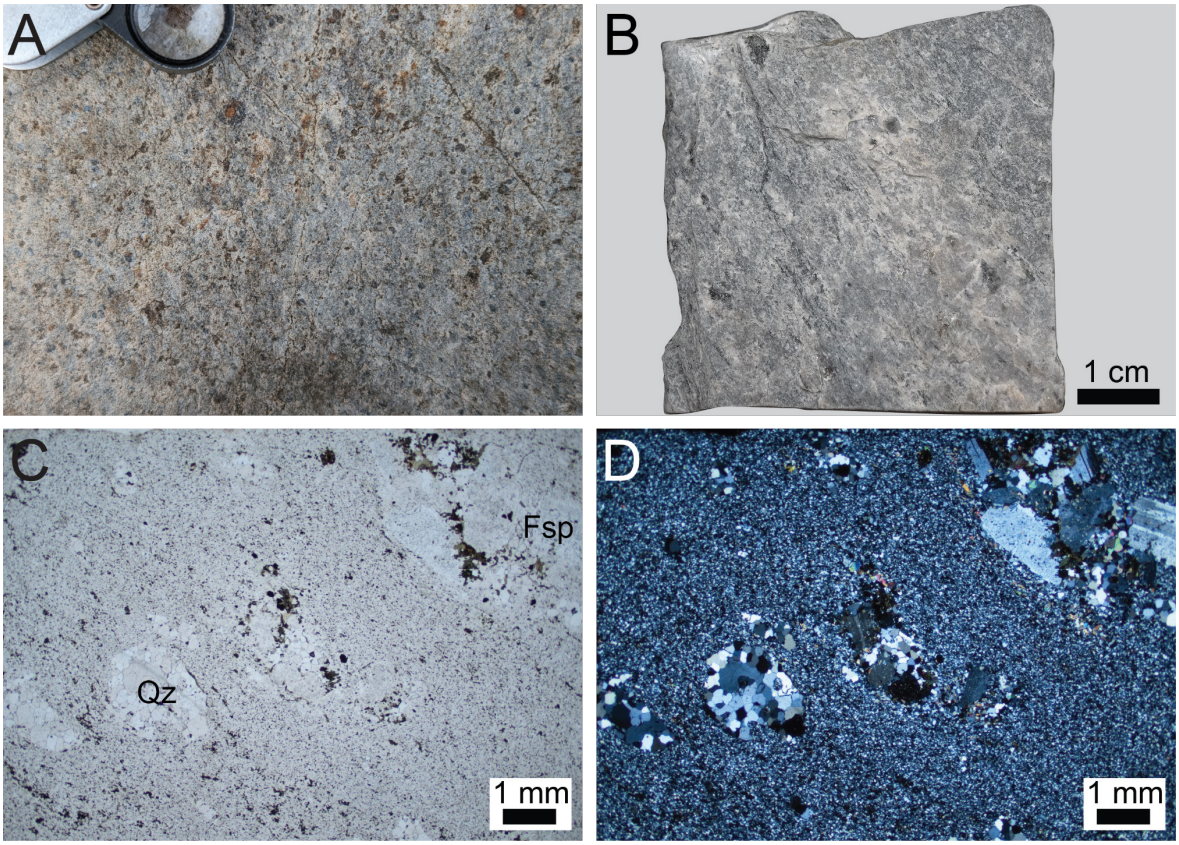

Figure 6. A. Photo of the porphyritic coherent unit sampled. Nordmark district. **B.** Photo of sample SAN240131A. **C–D.** Variably sized quartz phenocrysts with embayment texture (lower left) in a fine-grained groundmass. Thin section SAN240131A. Single-polarised light in C and cross-polarised light in D. Mineral abbreviations: Fsp = feldspar, Qz = quartz. Photos: Stefan Andersson.

Lithochemical data, obtained by ALS Global using Fusion decomposition followed by ICP-AES analysis, show the following major element concentrations (Andersson et al. 2025): 75.8 wt% SiO_2, 11.9 wt% Al_2O_3, 3.93 wt% Na_2O, 3.78 wt% K_2O, 0.70 wt% CaO, 2.70 wt% Fe_2O_3 and 0.46 wt% MgO. These results, together with the mineralogical characteristics, indicate that the metarhyolite is largely unaltered compared to nearby rocks affected by combined Na- and Fe-Mg-alteration processes (Andersson et al. 2025).

The extracted zircon grains from the analysed sample are subhedral to euhedral, showing elongate to stubby prismatic morphologies (fig. 7). They range from approximately 100 to 200 µm in length and 40 to 90 µm in width. Most zircons exhibit core-rim textures with distinct unzoned or faintly zoned cores overlain by oscillatory-zoned rims.

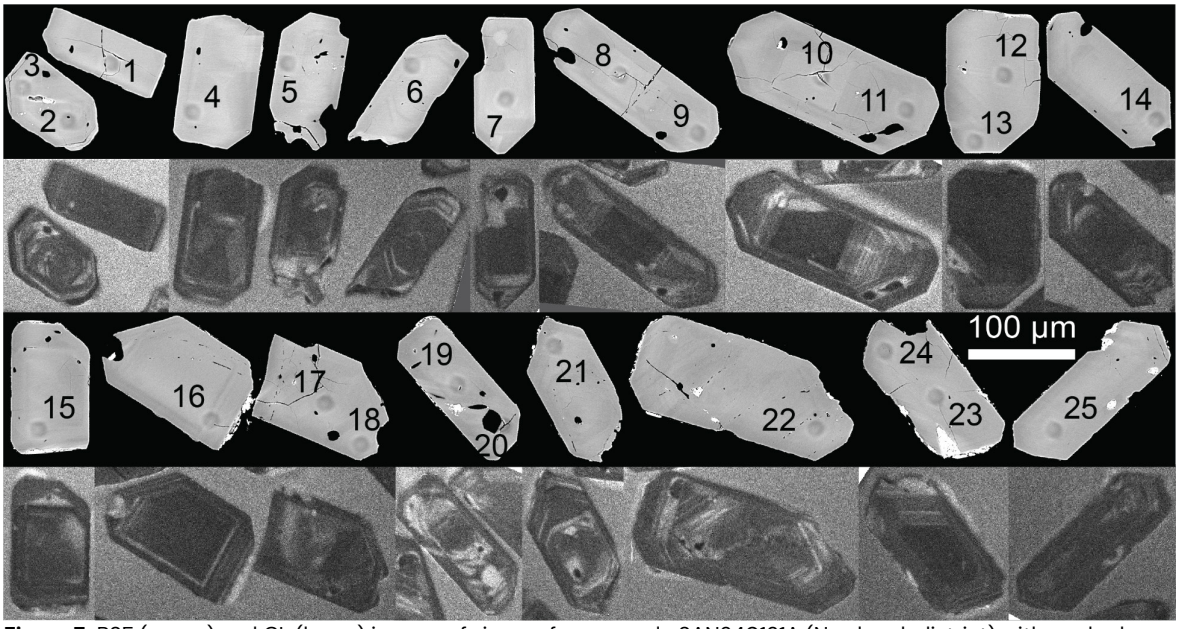

Figure 7. BSE (upper) and CL (lower) images of zircons from sample SAN240131A (Nordmark district) with marked analytical points. Brightest white in the BSE images is remnants of the gold coating. Photos: George Morris.

Result and interpretation of geochronological data

SAN230139A, Persberg

For this sample, 25 points from 14 different zircon crystals were analysed (Appendix 1). Eleven paired core and rim analyses were included to identify possible inherited cores or overgrowths. No systematic age difference was detected between cores and rims, indicating the absence of inherited components or secondary growth zones.

One analysis (16) is highly discordant and was excluded from all calculations and plots. Analyses 4, 5, 9, 18, and 19 also exhibit high discordance (> 3 % in conventional Wetherill concordia space) and were rejected. One analysis (8) yields a distinctly lower $^{207}Pb/^{206}Pb$ age (1873 ± 24 Ma). Excluding this analysis, a concordia can be calculated from the remaining data, giving an age of 1892 ± 3 Ma (n = 18; MSWD for concordance and equivalence of 1.4). However, the concordia plots slightly to the right of the concordia line, suggesting the inclusion of marginally discordant analyses. Applying a stricter concordance filter (< 1.0 % discordance) yields a refined concordia age of 1892.5 ± 4 Ma (n = 11; MSWD = 0.64), as shown in the Tera-Wasserburg diagram (fig. 8A).

This age overlaps within error with the weighted mean $^{207}Pb/^{206}Pb$ age of 1894.5 ± 3 Ma (24/25, MSWD = 1), excluding the single outlier (16) as calculated by IsoplotR (Vermeesch 2018). The concordia age of **1892.5 ± 4** Ma is interpreted as the best estimate for the crystallisation of the coherent volcanic unit in the Persberg ore district.

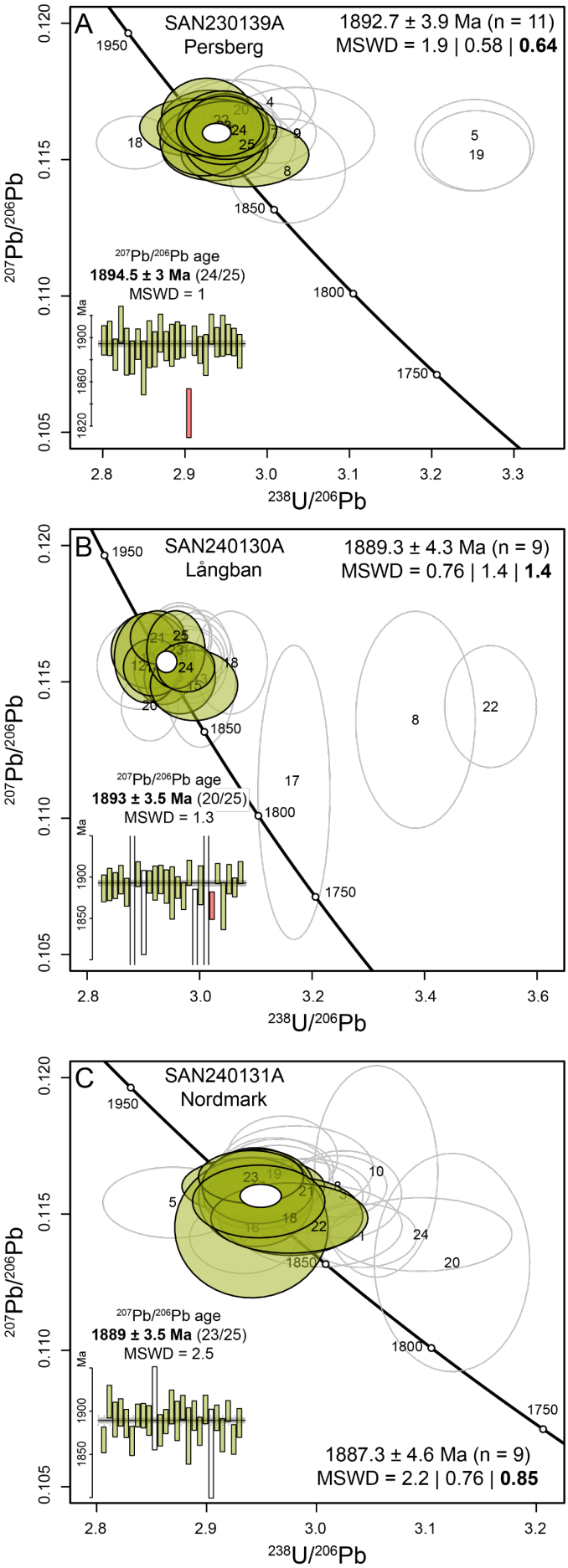

Figure 8. Tera-Wasserburg concordia diagrams with accompanying weighted mean $^{207}Pb/^{206}Pb$ age plots for zircon U–Pb analyses of the metarhyolite samples. **A.** Persberg (SAN230139A). **B.** Långban (SAN240130A). **C.** Nordmark (SAN240131A). Error ellipses are shown at the 2σ level. Rejected analyses (discordant or with large analytical uncertainties) are plotted as open ellipses.

SAN240130A, Långban

For this sample, 25 points from 17 different zircon crystals were analysed (Appendix 2). Six paired core and rim analyses were included to detect possible inherited cores or overgrowths. No systematic age differences between core and rim domains were observed, suggesting no inheritance or secondary zircon growth.

Two analyses (6 and 19) show very large analytical uncertainties and were excluded from all calculations and plots. One additional analysis (17) was discounted because of large $^{207}Pb/^{206}Pb$ ratio errors causing it to intersect the concordia at a lower apparent age (< 1800 Ma). Analyses 8, 18, and 22 show high discordance (> 3 %), and analysis 20 is reverse discordant; all were rejected.

The remaining 18 points define a concordant age of 1890 ± 3 Ma (n = 18; MSWD for concordance and equivalence of 1.9). The concordia lies slightly to the right of the concordia line, indicating inclusion of marginally discordant analyses. Applying a stricter concordance filter (< 1.5 % discordance) yields a refined concordia age of 1889.5 ± 4.5 Ma (n = 9; MSWD = 1.4), as shown in the Tera-Wasserburg diagram (fig. 8B).

This age overlaps within error with the weighted mean $^{207}Pb/^{206}Pb$ age of 1893 ± 3.5 Ma (20/25, MSWD = 1.3), excluding the four analyses with large errors (6, 8, 17, 19) and one outlier (20) as calculated using IsoplotR (Vermeesch 2018). The concordia age of **1889.5 ± 4.5** Ma is interpreted as the best estimate for the crystallisation of the coherent volcanic unit in the Långban ore district.

SAN240131A, Nordmark

For this sample, 25 points from 18 different zircon crystals were analysed (Appendix 3). Seven paired core and rim analyses were performed to test for inherited cores or overgrowths. No systematic age differences were identified, indicating the absence of inheritance or later zircon growth.

One analysis (20) shows very large errors and was excluded from all calculations. Analyses 3, 8, 10, and 24 are highly discordant (> 3 %), and analysis 5 is reverse discordant; all were rejected. Two analyses (1 and 6) also yield distinctly lower $^{207}Pb/^{206}Pb$ ages (1867 ± 15 Ma and 1865 ± 16 Ma, respectively). When these are excluded, the remaining data produce a concordia age of 1888 ± 3.5 Ma (n = 17; MSWD for concordance and equivalence of 1.8). The concordia plots slightly to the right of the concordia line, indicating the inclusion of slightly discordant spots. Applying a stricter concordance filter (< 1.0 % discordance) yields a refined concordia age of 1887.5 ± 4.5 Ma (n = 9; MSWD = 0.85), as shown in the Tera-Wasserburg diagram (fig. 8c).

This age overlaps within error with the weighted mean $^{207}Pb/^{206}Pb$ age of 1889 ± 3.5 Ma (23/25, MSWD = 2.5), excluding the two analyses with high uncertainties in the $^{207}Pb/^{206}Pb$ ratios (10 and 20). The $^{207}Pb/^{206}Pb$ ages may, however, define two age plateaus, one at ~1870 Ma (analyses 1, 6, 11, 16, 18, 22 and 24) and one at ~1895 Ma (analyses 2, 3, 4, 5, 7, 8, 9, 12, 13, 14, 15, 17, 19, 21, 23 and 25). Both spots include core and rim domains of the zircon crystals. This could explain the higher MSWD (fig. 8c), and slightly lower calculated ages compared to the other two districts. Nevertheless, the concordia age of **1887.5 ± 4.5** Ma is interpreted as the best estimate for the crystallisation of the coherent volcanic unit in the Nordmark ore district, acknowledging the wider spread in $^{207}Pb/^{206}Pb$ ages.

Discussion and conclusions

Although the dated metarhyolitic rocks were not sampled directly from the volcanic units intercalated with the marble-skarn sequences hosting the iron oxide ores, the coherent volcanic rocks occur in close proximity to them. In the Persberg ore district, the sampled coherent unit is located adjacent to skarn-altered volcanic siltstone–sandstone and iron oxide skarn ores at the Hallgruvorna ore field. This spatial association suggests that the lava or subvolcanic intrusion either postdates the skarn alteration or remained unaffected by it. In the Långban district, the targeted coherent unit shows both skarn and K-alteration and is situated just south of the main mines, in direct contact with the skarn-altered marble that hosts the Långban deposit. In the Nordmark district, the dated coherent unit lies next to the skarn-altered marble hosting the Nordmark ore field, yet the rock itself remains unaltered, again implying post-alteration emplacement or intrusion into a part of the system not subjected to skarn alteration. Taken together, these spatial and alteration relationships suggest that the dated volcanic rocks provide a reliable approximation of the timing of volcanic activity in each district.

The zircon U–Pb results from the three metarhyolite samples yield concordia ages that overlap within analytical uncertainty, 1892.5 ± 4 Ma for Persberg, 1889.5 ± 4.5 Ma for Långban, and 1887.5 ± 5 Ma for Nordmark. These ages, together with the overlapping $^{207}Pb/^{206}Pb$ ages of 1894.5 ± 3 Ma, 1893 ± 3.5 5 Ma and 1889 ± 3.5 Ma, respectively (fig. 8A–C), as well as the possible presence of two age clusters in the Nordmark $^{207}Pb/^{206}Pb$ population, indicate broadly coeval felsic volcanism at ca 1.89 Ga (fig. 9A–B). While minor age differences between districts (e.g., Nordmark) cannot be ruled out, the age uncertainties (~5 Ma) preclude resolving such small offsets. Therefore, despite potential stratigraphic separation, the volcanic–volcanosedimentary successions in Persberg, Långban, and Nordmark are interpreted to occupy broadly equivalent stratigraphic positions. This interpretation is supported by shared primary features of the volcanic wall rocks, including similar textures and overall appearance (Andersson et al. 2025). The temporal overlap of these volcanic rocks suggests that both the Mn-poor skarn system (Persberg) and the Mn-rich system (Långban) formed within broadly contemporaneous submarine volcanic–sedimentary environments. The presence of mixed Mn-poor and Mn-rich skarn systems in Nordmark further supports this conclusion.

These findings refine the regional volcanic framework of western Bergslagen and demonstrate that volcanism and ore formation in the classical districts of Persberg, Långban, and Nordmark were active during the volcanic stage at ca 1.89 Ga coeval with the plutonic-subvolcanic activity forming the major GSD granitic-subvolcanic unit in the region ("Horssjö granite"; 1892 ± 8 Ma, Andersen et al. 2009). This aligns with the timing of major base metal ore formation across Bergslagen, mostly sulphide-dominated skarn ores but also various Fe oxide ores hosted in skarn or carbonate rocks in ore districts such as Garpenberg, Falun, and Stollberg. These deposits are similarly associated with proximal volcanic settings and are temporally linked to the voluminous volcanic and plutonic activity during this period (Jansson & Allen 2011; Jansson et al. 2013, 2023; Kampmann et al. 2016; Stephens & Jansson 2020).

A broader regional perspective reinforces this interpretation. A compilation of zircon U–Pb ages from volcanic rocks across the Bergslagen ore province, presented as frequency histograms and probability density curves (fig. 9A–B), reveals two principal volcanic pulses: one at approximately 1905 Ma and another, more dominant at 1894 Ma. The ages from Persberg, Långban, and Nordmark fall within the younger pulse, suggesting that these districts were part of a widespread felsic volcanic event. This supports the interpretation that the volcano-sedimentary successions in these districts are not only stratigraphically equivalent but also genetically linked to the same regional magmatic system.

In conclusion, the integrated geochronological and geological data from this study contribute to a more coherent model of volcanic and ore-forming processes in western Bergslagen. The broadly coeval nature of volcanism across the Persberg, Långban, and Nordmark districts, coupled with similar primary volcanic lithologies and textures, supports a proximal, volcanic–sedimentary ore-forming environment active around 1.89 Ga, coeval with associated plutonic–subvolcanic activity.

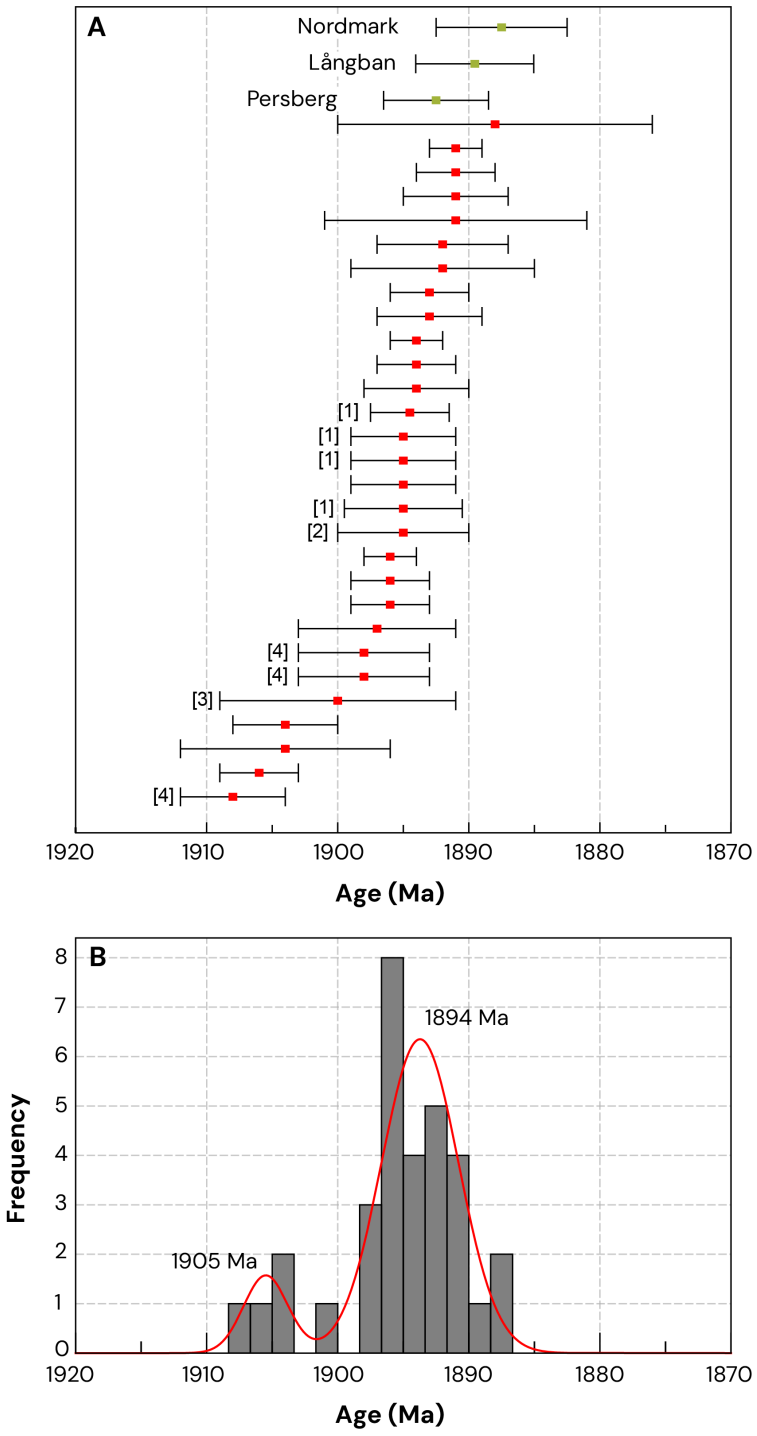

Figure 9. A. Compilation of zircon U–Pb ages for volcanism in the Bergslagen ore province (lithotectonic unit). The ages for the Persberg, Långban and Nordmark districts from this study are shown in green. **B**. Histograms of volcanic crystallisation zircon U–Pb ages. Grey bars show the frequency distribution of individual age determinations, and the red line represents a fitted two-component Gaussian mixture model of the probability density curve. The diagram reveals two main volcanic pulses at ca 1905 Ma and ca 1894 Ma. Both diagrams are based on the age compilation of Stephens & Jansson (2020) with additional data from [1], [2], Kuipers et al. (2018, 2021), [3], Lewerentz et al. (2021) and [4], Jansson et al. (2023). The frequency distribution diagram also includes data from this study.

References

Andersen, T., Andersson, U.B., Graham, S., Åberg, G., Simonsen, S.L., 2009: Granitic magmatism by melting of juvenile continental crust: new constraints on the source of Palaeoproterozoic granitoids in Fennoscandia from Hf isotopes in zircon. *Journal of the Geological Society 166*, 233–247.

Andersson, S., Brolin, C., Lewerentz, A. & Camitz, J., 2025: Bergslagen etapp 3. Malmnära kartering i området Persberg–Nordmark 2022–2024. *SGU-rapport 2025:12*, Sveriges geologiska undersökning, 101 pp.

Bergman, S., Stephens, M.B., Andersson, J., Kathol, B. & Bergman, T., 2012: Sveriges berggrund, skala 1:1 miljon. *Sveriges geologiska undersökning K 423*.

Björk, L., 1986: Beskrivning till berggrundskartan Filipstad NV. *Sveriges geologiska undersökning Af 147*, 110 pp.

Boström, K., Rydell, H. & Joensuu, O., 1979: Långban – an exhalative sedimentary deposit? *Economic Geology 74*, 1002–1011.

Holtstam, D. & Langhof, J. (Eds.), 1999: *Långban, the mines, their minerals, geology and explorers*. Raster förlag, Stockholm, 215 pp.

Holtstam, D. & Mansfeld, J., 2001: Origin of a carbonate-hosted Fe-Mn-(Ba-As-Pb-Sb-W) deposit of Långban-type in Central Sweden. *Mineralium Deposita 36*, 641–657.

Jansson, N.F. & Allen, R.L., 2011: Timing of volcanism, hydrothermal alteration and ore formation at Garpenberg, Bergslagen, Sweden. *GFF 133*, 3–18.

Jansson, N.F., Erismann, F., Lundstam, E. & Allen, R.L., 2013: Evolution of the Paleoproterozoic volcanic-limestone-hydrothermal sediment succession and Zn-Pb-Ag and iron oxide deposits at Stollberg, Bergslagen region, Sweden. *Economic Geology 108*, 309–335.

Jansson, N.F., Simán, F., Allen, R.L., Mansfeld, J. & Kampmann, T.C., 2023: Age constraints on c. 1.9 Ga volcanism, basin evolution and mineralization at the world-class Zinkgruvan Zn-Pb-Ag(-Cu) deposit, Bergslagen, Sweden. *Precambrian Research 395*, 107131.

Jonsson, E., 2004: Fissure mineral formation and metallogenesis in the Långban Fe-Mn-(Ba-As-Pb-Sb…) deposit, Bergslagen, Sweden. *Meddelanden från Stockholms Universitets Institution för Geologi och geokemi 318*, 22 pp.

Kampmann, T.C., Stephens, M.B., Ripa, M., Hellström, F.A. & Majka, J., 2016: Time constraints on magmatism, mineralisation and metamorphism at the Falun base metal sulphide deposit, Sweden, using U-Pb geochronology on zircon and monazite. *Precambrian Research 278*, 52–68.

Kuipers, G., Beunk, F.F., Yi, K. & van der Wateren, F.M., 2018: The Palaeoproterozoic Grythyttan field in the Svecofennian orogen, west Bergslagen, central Sweden: structure, stratigraphy and age. *Norwegian Journal of Geology 98*, 333–357.

Kuipers, G., Beunk, F.F., Yi, K. & van der Wateren, F.M., 2021: A 1.9 Ga glacial sedimentary-facies association at low palaeolatitude in the Bergslagen Group, Grythyttan Field, Central Sweden. *Norwegian Journal of Geology 101*, 202101.

Lewerentz, A., Ripa, M. & Morris, G., 2021: Time constraints on the deposition of a mineralisation-proximal metavolcaniclastic rock at Byngsbodberget, northwest of Falun, Bergslagen, Sweden. *GFF 143*, 321–327.

Magnusson, N.H., 1925: Persbergs malmtrakt och berggrunden i de centrala delarna av Filipstads bergslag. *Kungliga Kommerskollegium, Beskrivningar över mineralfyndigheter nr. 2*, 239 pp.

Magnusson, N.H., 1929: Nordmarks malmtrakt. *Sveriges geologiska undersökning Ca 13*, 90 pp.

Magnusson, N.H., 1930: Långbans malmtrakt. *Sveriges geologiska undersökning Ca 23*, 111 pp.

Petersson, W., 1896: Nordmarks grufvors Odalfält. *Sveriges geologiska undersökning C 162*, 60 pp.

Sjögren, H., 1910: The Långban mines. *Geologiska Föreningens i Stockholm Förhandlingar 13*, 373–435.

Stacey, J.S. & Kramers, J.D., 1975: Approximation of terrestrial lead isotope evolution by a two-stage model. *Earth and Planetary Science Letters 26*, 207–221.

Steiger, R.H. & Jäger, E., 1977: Convention on the use of decay constants in geo- and cosmochronology. *Earth and Planetary Science Letters 36*, 359–362.

Stephens, M.B. & Jansson, N.F., 2020: Chapter 6: Paleoproterozoic (1.9–1.8 Ga) synorogenic magmatism, sedimentation and mineralization in the Bergslagen lithotectonic unit, Svecokarelian orogen. *In:* M.B. Stephens & J. Bergman Weihed (Eds.): Sweden: lithotectonic framework, tectonic evolution and mineral resources. *Geological Society of London Memoirs 50*, 105–206.

Stephens, M.B., Ripa, M., Lundström, I., Persson, L., Bergman, T., Ahl, M., Wahlgren, C.-H., Persson, P.-O. & Wickström, L., 2009: Synthesis of the bedrock geology in the Bergslagen region, Fennoscandian Shield, south-central Sweden. *Sveriges geologiska undersökning Ba 58*, 259 pp.

Törnebohm, A.E., 1875: Geognostisk beskrifning öfver Persbergets grufvefält. *Sveriges geologiska undersökning C 14*, 21 pp.

Welin, E., 1987: The depositional evolution of the Svecofennian supracrustal sequence in Finland and Sweden. *Precambrian Research 35*, 95–113.

Whitehouse, M., J. & Kamber, B.S., 2005: Assigning dates to thin gneissic veins in high-grade metamorphic terranes: A cautionary tale from Akilia, Southwest Greenland. *Journal of Petrology 46*, 291–318.

Whitehouse, M.J., Claesson, S., Sunde, T. & Vestin, J., 1997: Ion-microprobe U–Pb zircon geochronology and correlation of Archaean gneisses from the Lewisian Complex of Gruinard Bay, north-west Scotland. *Geochimica et Cosmochimica Acta 61*, 4429–4438.

Whitehouse, M.J., Kamber, B.S. & Moorbath, S., 1999: Age significance of U–Th–Pb zircon data from Early Archaean rocks of west Greenland: a reassessment based on combined ion-microprobe and imaging studies. *Chemical Geology (Isotope Geoscience Section) 160*, 201–224.

Wiedenbeck, M., Allé, P., Corfu, F., Griffin, W.L., Meier, M., Oberli, F., Quadt, A.V., Roddick, J.C. & Spiegel, W., 1995: Three natural zircon standards for U-Th-Pb, Lu-Hf, trace element and REE analyses. *Geostandards Newsletter 19*, 1–23.

Wiedenbeck, M., Hanchar, J.M., Peck, W.H., Sylvester, P., Valley, J., Whitehouse, M., Kronz, A., Morishita, Y., Nasdala, L., Fiebig, J., Franchi, I., Girard, J.P., Greenwood, R.C., Hinton, R., Kita, N., Mason, P.R.D., Norman, M., Ogasawara, M., Piccoli, P.M., Rhede, D., Satoh, H., Schulz-Dobrick, B., Skår, O., Spicuzza, M.J., Terada, K., Tindle, A., Togashi, S., Vennemann, T., Xie, Q. & Zheng, Y.F., 2004: Further characterisation of the 91500 zircon crystal. *Geostandards and Geoanalytical Research 28*, 9–39.

Vermeesch, P., 2018, IsoplotR: a free and open toolbox for geochronology. *Geoscience Frontiers 9*, 1479–1493.

Appendix 1. U–Pb zircon data for sample SAN230139A

Analysis point	Core–rim pairs	$^{238}U/^{206}Pb$	±σ (%)	$^{207}Pb/^{206}Pb$	±σ (%)	Disc. % Conv.	Disc. % 2s lim.	$^{207}Pb/^{235}U$	±σ (%)	$^{206}Pb/^{238}Pb$	±σ (%)	ρ	$^{208}Pb/^{232}U$	±σ (%)	$^{207}Pb/^{206}Pb$ age (Ma)	±σ	$^{206}Pb/^{238}U$ age (Ma)	±σ	U (ppm)	Th (ppm)	Pb (ppm)	Th/U (calc)	Th/U (meas.)
1	core	2.91290	0.93901	0.11618	0.36986	0.26		5.49941	1.00923	0.34330	0.93901	0.93043	0.09996	4.94706	1897.5	6.6	1902.5	15.5	301.7	147.6	130.3	0.50	0.49
2	rim	2.92972	0.81593	0.11630	0.43005	-0.43		5.47333	0.92232	0.34133	0.81593	0.88465	0.10065	1.70321	1899.3	7.7	1893.1	13.4	228.8	79.6	95.2	0.36	0.35
3	core	2.93651	0.88176	0.11535	0.39089	0.24		5.41618	0.96451	0.34054	0.88176	0.91420	0.09792	1.65461	1884.6	7	1889.3	14.4	279.7	122.1	118.2	0.44	0.44
4	rim	3.00382	0.73507	0.11712	0.45759	-3.62	-1.1	5.37600	0.86586	0.33291	0.73507	0.84895	0.09783	1.67941	1911.9	8.2	1852.5	11.8	204.7	64.8	82.5	0.32	0.32
5		3.25198	0.89267	0.11552	0.58567	-9.64	-6.5	4.89811	1.06764	0.30750	0.89267	0.83611	0.08462	2.09951	1887.3	10.5	1728.4	13.5	150.8	66	57.3	0.42	0.44
6	core	2.97305	1.05096	0.11519	0.41456	-0.84		5.34201	1.12977	0.33635	1.05096	0.93025	0.09769	1.74878	1882.0	7.5	1869.1	17.1	244.5	98.8	101.4	0.41	0.40
7	rim	3.00892	0.67733	0.11596	0.38215	-2.74	-0.5	5.31368	0.77770	0.33234	0.67733	0.87094	0.09679	1.52734	1894.0	6.9	1849.7	10.9	296.7	112.9	121	0.39	0.38
8		3.02451	0.93966	0.11458	0.67105	-1.96		5.22359	1.15467	0.33063	0.93966	0.81379	0.09710	2.95511	1872.5	12.1	1841.4	15.1	99.4	39.8	40.5	0.41	0.40
9	core	3.03634	1.24600	0.11595	0.58837	-3.61		5.26548	1.37793	0.32934	1.24600	0.90426	0.08158	2.17833	1894.0	10.6	1835.2	19.9	125	39.2	49.1	0.27	0.31
10	rim	2.92279	0.73122	0.11567	0.43862	0.41		5.45643	0.85268	0.34214	0.73122	0.85755	0.09681	1.71436	1889.5	7.9	1897.0	12.0	221.4	78.5	92.1	0.35	0.35
11	core	2.92701	0.76239	0.11660	0.47612	-0.62		5.49279	0.89885	0.34165	0.76239	0.84819	0.09880	1.68456	1904.0	8.6	1894.6	12.5	185	77.8	78.2	0.42	0.42
12	rim	2.96295	0.65558	0.11585	0.36396	-1.12		5.39086	0.74984	0.33750	0.65558	0.8743	0.09856	1.53479	1892.3	6.5	1874.6	10.7	322.5	125.8	133.8	0.40	0.39
13	core	2.94778	0.70338	0.11590	0.52654	-0.66		5.42100	0.87863	0.33924	0.70338	0.80054	0.09969	1.56913	1893.1	9.5	1883.0	11.5	270	121.3	114.3	0.46	0.45
14	rim	2.94621	0.76977	0.11617	0.46763	-0.86		5.43666	0.90068	0.33942	0.76977	0.85465	0.09879	1.59478	1897.3	8.4	1883.9	12.6	286.2	106.6	119	0.38	0.37
15	core	2.95381	0.87066	0.11612	0.41047	-1.07		5.42033	0.96256	0.33855	0.87066	0.90452	0.09807	1.74165	1896.5	7.4	1879.7	14.2	250.3	109.5	105.3	0.44	0.44
16	rim	6.61751	5.36401	0.11202	0.60808	-54.04	-48.3	2.33408	5.39837	0.15111	5.36401	0.99364	0.01945	9.02789	1831.7	11	907.20	45.4	312.2	209	56.5	0.30	0.67
17	core	2.93430	0.93000	0.11616	0.36710	-0.46		5.45846	0.99983	0.34080	0.93000	0.93016	0.09709	1.68294	1897.2	6.6	1890.5	15.2	307.4	137.9	130.3	0.44	0.45
18	rim	2.83906	0.66090	0.11563	0.33674	3.41	1.3	5.61542	0.74174	0.35223	0.66090	0.89101	0.10145	1.47964	1888.9	6.1	1945.2	11.1	384	162.2	167.3	0.42	0.42
19	core	3.25419	0.81279	0.11533	0.51204	-9.53	-6.8	4.88648	0.96063	0.30730	0.81279	0.84610	0.08545	1.73673	1884.2	9.2	1727.4	12.3	194	77.7	73.1	0.39	0.40
20	rim	2.96857	0.98063	0.11684	0.37675	-2.23		5.42678	1.05051	0.33686	0.98063	0.93348	0.09918	1.72742	1907.6	6.8	1871.6	15.9	333.4	146.8	140	0.45	0.44
21	core	2.95060	0.83078	0.11608	0.36905	-0.92		5.42415	0.90906	0.33891	0.83078	0.91389	0.09797	1.57505	1895.8	6.6	1881.4	13.6	315.3	144	133.4	0.46	0.46
22	rim	2.94413	0.87237	0.11646	0.51388	-1.06		5.45401	1.01247	0.33966	0.87237	0.86162	0.09735	1.66677	1901.8	9.2	1885.0	14.3	257.8	88.1	106.3	0.34	0.34
23	core	2.94765	0.65021	0.11623	0.38086	-0.97		5.43682	0.75354	0.33925	0.65021	0.86287	0.09719	1.50317	1898.2	6.8	1883.1	10.6	299.3	131.6	126.1	0.44	0.44
24	rim	2.96592	0.69211	0.11608	0.34471	-1.44		5.39652	0.77321	0.33716	0.69211	0.89512	0.09756	1.53753	1896.0	6.2	1873.0	11.2	390.6	155	162.1	0.40	0.40
25		2.97535	0.79847	0.11555	0.42101	-1.25		5.35452	0.90266	0.33610	0.79847	0.88457	0.09602	1.66984	1887.6	7.6	1867.9	12.9	249.6	111.4	104.3	0.44	0.45

Appendix 2. U–Pb zircon data for sample SAN240130A

Analysis point	Core-rim pairs	$^{238}U/^{206}Pb$	±σ (%)	$^{207}Pb/^{206}Pb$	±σ (%)	Disc. % Conv.	Disc. % 2s lim.	$^{207}Pb/^{235}U$	±σ (%)	$^{206}Pb/^{238}Pb$	±σ (%)	ρ	$^{208}Pb/^{232}U$	±σ (%)	$^{207}Pb/^{206}Pb$ age (Ma)	±σ	$^{206}Pb/^{238}U$ age (Ma)	±σ	U (ppm)	Th (ppm)	Pb (ppm)	Th/U (calc)	Th/U (meas.)
1		2.93591	0.72488	0.11546	0.45116	0.15		5.42248	0.85381	0.34061	0.72488	0.84899	0.09811	1.58755	1886.3	8.1	1889.6	11.9	221.2	95.8	93.4	0.43	0.43
2		2.98720	0.85193	0.11577	0.54128	-1.86		5.34367	1.00934	0.33476	0.85193	0.84405	0.09755	1.86171	1891.1	9.7	1861.4	13.8	147.7	46.9	59.7	0.32	0.32
3	core	2.98394	0.76176	0.11568	0.43492	-1.66		5.34513	0.87718	0.33513	0.76176	0.86843	0.09765	1.76995	1889.6	7.8	1863.2	12.3	250.4	124.8	105.8	0.50	0.50
4	rim	2.91116	0.94257	0.11614	0.47942	0.36		5.50052	1.05749	0.34351	0.94257	0.89133	0.09787	1.78504	1896.8	8.6	1903.5	15.5	197.4	66	82.2	0.33	0.33
5	core	2.96488	0.85980	0.11516	0.46943	-0.54		5.35568	0.97960	0.33728	0.85980	0.87771	0.09681	1.74639	1881.7	8.5	1873.6	14	239	104.8	100	0.44	0.44
6	rim	2.99227	2.53313	0.11918	7.31105	-5.05		5.49170	7.73745	0.33419	2.53313	0.32739	0.09555	19.1393	1943.2	131	1858.7	40.9	231.6	101.3	96.3	0.44	0.44
7	core	2.96425	0.78191	0.11657	0.41693	-1.83		5.42202	0.88612	0.33735	0.78191	0.88240	0.09781	1.88081	1903.4	7.5	1873.9	12.7	248.1	105.5	103.8	0.43	0.43
8	rim	3.38397	1.26433	0.11361	1.40940	-11.53	-4.7	4.62897	1.89339	0.29551	1.26433	0.66776	0.07642	4.03224	1857.1	25.5	1669.0	18.6	372.8	144.7	133.7	0.35	0.39
9	core	2.97312	0.95465	0.11596	0.37651	-1.57		5.37786	1.02621	0.33635	0.95465	0.93026	0.09709	1.76275	1894.1	6.8	1869.1	15.5	308	132.3	128.5	0.43	0.43
10	rim	2.90763	0.82073	0.11588	0.57497	0.73		5.49501	1.00209	0.34392	0.82073	0.81902	0.08400	3.13485	1892.8	10.3	1905.5	13.5	284.9	126	119.9	0.38	0.44
11	core	2.98175	0.98529	0.11616	0.47714	-2.03		5.37121	1.09474	0.33537	0.98529	0.90002	0.09833	1.87809	1897.1	8.6	1864.4	16	189.5	61.7	77	0.33	0.33
12	rim	2.89092	1.01949	0.115600	0.55861	1.57		5.51368	1.16250	0.34591	1.01949	0.87698	0.09695	2.13902	1888.5	10.1	1915.0	16.9	156.6	48.9	65.2	0.30	0.31
13		3.00087	0.84454	0.11511	0.87826	-1.69		5.28894	1.21843	0.33324	0.84454	0.69314	0.09765	2.23990	1880.8	15.8	1854.0	13.6	176.8	63.2	71.9	0.36	0.36
14		2.91692	0.72119	0.11553	0.36463	0.74		5.46087	0.80813	0.34283	0.72119	0.89242	0.09986	1.58011	1887.3	6.6	1900.3	11.9	405.5	176	172.7	0.44	0.43
15		2.99003	1.04616	0.11487	0.45280	-1.10		5.29703	1.13995	0.33444	1.04616	0.91773	0.09311	1.93170	1877.0	8.2	1859.9	16.9	251.7	85.5	101.8	0.33	0.34
16		2.96423	0.73423	0.11668	0.42125	-1.94		5.42738	0.84649	0.33736	0.73423	0.86739	0.09965	1.68786	1905.2	7.6	1873.9	11.9	241.6	103.9	101.4	0.44	0.43
17	core	3.16792	0.81256	0.11095	1.95826	-2.92		4.82876	2.12015	0.31566	0.81256	0.38325	0.09187	5.70215	1814.1	35.6	1768.5	12.6	307.6	113.9	118.3	0.37	0.37
18	rim	3.05501	0.86072	0.11570	0.65550	-3.97	-0.5	5.22199	1.08190	0.32733	0.86072	0.79556	0.09348	2.00045	1890.1	11.8	1825.4	13.7	126.7	37.1	49.8	0.29	0.29
19		3.26022	2.55868	0.09982	13.0932	7.30		4.22158	13.3409	0.30673	2.55868	0.19179	0.05143	62.1633	1619.9	244	1724.6	38.7	279.1	95.7	99.1	0.20	0.34
20		2.91128	0.70225	0.11414	0.46048	2.30		5.40552	0.83976	0.34349	0.70225	0.83625	0.09839	1.66131	1865.5	8.3	1903.4	11.6	207.9	75	86.9	0.36	0.36
21		2.92539	0.66784	0.11662	0.33745	-0.58		5.49676	0.74825	0.34184	0.66784	0.89253	0.09917	1.59479	1904.3	6.1	1895.5	11	374.4	178.7	160.6	0.48	0.48
22		3.51743	0.93418	0.11409	0.78900	-15.29	-11.3	4.47232	1.22279	0.28430	0.93418	0.76397	0.08664	2.44248	1864.8	14.2	1613.0	13.3	373.9	141.9	130.7	0.40	0.38
23		2.95795	0.70543	0.11618	0.49465	-1.26		5.41543	0.86157	0.33807	0.70543	0.81877	0.09670	1.87893	1897.4	8.9	1877.4	11.5	177.3	56.7	72.4	0.32	0.32
24		2.97585	0.69111	0.11553	0.31620	-1.26		5.35301	0.76001	0.33604	0.69111	0.90934	0.09824	1.48086	1887.4	5.7	1867.6	11.2	493.7	241.7	208.8	0.50	0.49
25		2.96673	0.74821	0.11669	0.37158	-2.03		5.42336	0.83540	0.33707	0.74821	0.89563	0.09640	2.26420	1905.4	6.7	1872.6	12.2	365.8	198.3	156.8	0.54	0.54

Appendix 3. U–Pb zircon data for sample SAN240131A

Analysis point	Core-rim pairs	$^{238}U/^{206}Pb$	±σ (%)	$^{207}Pb/^{206}Pb$	±σ (%)	Disc. % Conv.	Disc. % 2s lim.	$^{207}Pb/^{235}U$	±σ (%)	$^{206}Pb/^{238}Pb$	±σ (%)	ρ	$^{208}Pb/^{232}U$	±σ (%)	$^{207}Pb/^{206}Pb$ age (Ma)	±σ	$^{206}Pb/^{238}U$ age (Ma)	±σ	U (ppm)	Th (ppm)	Pb (ppm)	Th/U (calc)	Th/U (meas.)
1		3.04133	0.66198	0.11421	0.41204	-2.15		5.17786	0.77974	0.32880	0.66198	0.84898	0.09602	1.64004	1866.7	7.4	1832.6	10.6	369.4	163.8	151.1	0.45	0.44
2	core	2.96898	0.6796	0.11706	0.52646	-2.44		5.43635	0.85966	0.33682	0.6796	0.79054	0.09738	1.61672	1911.0	9.5	1871.3	11	201.4	76.9	83.3	0.38	0.38
3	rim	3.02418	0.70889	0.11572	0.55698	-3.01	-0.1	5.27591	0.90153	0.33067	0.70889	0.78632	0.09758	1.56934	1890.3	10	1841.6	11.4	238.1	96.9	97.3	0.42	0.41
4		2.96470	0.68507	0.11625	0.43951	-1.56		5.40648	0.81393	0.33730	0.68507	0.84168	0.09681	1.63541	1898.5	7.9	1873.7	11.1	219.6	82.1	90.6	0.37	0.37
5		2.86929	0.89058	0.11542	0.45337	2.51		5.54659	0.99934	0.34852	0.89058	0.89117	0.10027	1.70712	1885.7	8.2	1927.5	14.8	214.1	92.3	92.5	0.43	0.43
6		2.93362	0.67192	0.11414	0.46743	1.52		5.36457	0.81852	0.34088	0.67192	0.8209	0.09705	1.64569	1865.5	8.4	1890.9	11	216.7	81.5	90.2	0.37	0.38
7		2.94250	0.88785	0.11602	0.36895	-0.60		5.43640	0.96145	0.33985	0.88785	0.92344	0.09914	1.64740	1894.9	6.6	1885.9	14.5	304.1	136.7	128.9	0.46	0.45
8	core	3.01929	0.59726	0.11601	0.39333	-3.11	-1.0	5.29758	0.71514	0.33120	0.59726	0.83517	0.09621	1.59244	1894.8	7.1	1844.2	9.6	395.5	193.9	164.8	0.50	0.49
9	rim	2.97633	0.89199	0.11565	0.47628	-1.38		5.35753	1.01118	0.33598	0.89199	0.88213	0.09584	1.74376	1889.2	8.6	1867.3	14.5	190.3	65.4	77.6	0.34	0.34
10	core	3.05435	0.73981	0.11656	1.33951	-4.72		5.26169	1.53023	0.32740	0.73981	0.48346	0.09297	2.73453	1903.3	24.1	1825.8	11.8	401.4	190.9	164.5	0.47	0.48
11	rim	2.97626	0.89149	0.11492	0.50332	-0.69		5.32386	1.02376	0.33599	0.89149	0.8708	0.09747	1.77716	1877.8	9.1	1867.4	14.5	202.4	70.6	82.7	0.35	0.35
12	core	2.94691	0.67515	0.11557	0.39000	-0.32		5.40730	0.77969	0.33934	0.67515	0.86591	0.09829	1.47337	1888.0	7	1883.5	11	400.9	184.4	169.9	0.46	0.46
13	rim	2.98122	0.94916	0.11666	0.54406	-2.47		5.39529	1.09404	0.33543	0.94916	0.86758	0.09739	1.95071	1904.8	9.8	1864.7	15.4	210.9	78.9	86.7	0.38	0.37
14		2.94468	0.70878	0.11562	0.63000	-0.29		5.41355	0.94830	0.33960	0.70878	0.74742	0.09909	1.74191	1888.7	11.3	1884.7	11.6	201.9	66.9	83.1	0.34	0.33
15		2.96601	0.67299	0.11663	0.38632	-1.95		5.42177	0.77599	0.33715	0.67299	0.86727	0.09644	1.53535	1904.4	6.9	1873.0	10.9	278	109.4	115.2	0.39	0.39
16		2.94083	0.95465	0.1145	0.90425	0.91		5.36844	1.31492	0.34004	0.95465	0.72602	0.11125	2.99097	1871.3	16.3	1886.9	15.6	187.8	63.3	78.2	0.38	0.34
17	core	2.94675	0.69279	0.11601	0.47307	-0.73		5.42821	0.83890	0.33936	0.69279	0.82583	0.09822	2.00623	1894.8	8.5	1883.6	11.3	187.2	67.7	77.6	0.36	0.36
18	rim	2.97535	0.96641	0.11485	0.45110	-0.59		5.32223	1.06651	0.33610	0.96641	0.90615	0.09721	1.78641	1876.7	8.1	1867.9	15.7	215.9	75.4	88.2	0.35	0.35
19	core	2.96108	0.69245	0.11647	0.46013	-1.64		5.42337	0.83139	0.33771	0.69245	0.83288	0.09709	1.59209	1901.9	8.3	1875.7	11.3	279.6	127.9	117.8	0.46	0.46
20	rim	3.12348	0.91197	0.11322	1.42266	-3.78		4.99767	1.68987	0.32016	0.91197	0.53967	0.10108	4.34386	1850.8	25.7	1790.5	14.3	150.3	45.7	58.2	0.33	0.30
21		2.99113	0.77557	0.11585	0.40859	-2.06		5.34029	0.87662	0.33432	0.77557	0.88473	0.09725	1.61982	1892.3	7.4	1859.3	12.5	268.5	106.5	110.5	0.40	0.40
22		3.00223	1.01608	0.11456	0.52826	-1.20		5.26105	1.14520	0.33309	1.01608	0.88725	0.09940	2.01212	1872.1	9.5	1853.3	16.4	157.0	44.7	62.7	0.29	0.28
23	core	2.94046	0.65442	0.11636	0.33500	-0.84		5.45604	0.73518	0.34008	0.65442	0.89015	0.09692	1.46512	1900.2	6	1887.1	10.7	404.4	194.1	172.3	0.48	0.48
24	rim	3.09502	1.07786	0.11425	0.47445	-3.88	-0.9	5.08966	1.17766	0.32310	1.07786	0.91526	0.09596	2.07215	1867.3	8.6	1804.8	17	221.8	73.1	86.9	0.34	0.33
25		2.94746	0.82282	0.11546	0.46480	-0.24		5.40116	0.94503	0.33928	0.82282	0.87068	0.09858	1.84756	1886.3	8.4	1883.2	13.4	214.3	84.3	89.4	0.40	0.39